

ENSO phase-locking to the boreal winter in CMIP3 and CMIP5 models

Yoo-Geun Ham · Jong-Seong Kug

Received: 28 February 2013 / Accepted: 21 January 2014 / Published online: 8 February 2014
© Springer-Verlag Berlin Heidelberg 2014

Abstract In this study, the El Niño-Southern Oscillation (ENSO) phase-locking to the boreal winter in CMIP3 and CMIP5 models is examined. It is found that the models that are poor at simulating the winter ENSO peak tend to simulate colder seasonal-mean sea-surface temperature (SST) during the boreal summer and associated shallower thermocline depth over the eastern Pacific. These models tend to amplify zonal advection and thermocline depth feedback during boreal summer. In addition, the colder eastern Pacific SST in the model can reduce the summertime mean local convective activity, which tends to weaken the atmospheric response to the ENSO SST forcing. It is also revealed that these models have more serious climatological biases over the tropical Pacific, implying that a realistic simulation of the climatological fields may help to simulate winter ENSO peak better. The models that are poor at simulating ENSO peak in winter also show excessive anomalous SST warming over the western Pacific during boreal winter of the El Niño events, which leads to strong local convective anomalies. This prevents the southward shift of El Niño-related westerly during boreal winter season. Therefore, equatorial westerly is prevailed over the western Pacific to further development of ENSO-related SST during boreal winter. This bias in the SST anomaly is partly due to the climatological dry biases over the central Pacific, which confines ENSO-related

precipitation and westerly responses over the western Pacific.

Keywords ENSO · Phase Locking · CMIP models

1 Introduction

The coupling between the seasonal cycle and the El Niño-Southern Oscillation (ENSO) was examined decades ago to highlight the role of seasonal evolution in the basic state in the ENSO evolution (Jin et al. 1994). The peak phase of the ENSO tends to appear in the boreal winter; this ENSO phase-locking in winter is considered as a typical feature of interaction between seasonal cycle and ENSO. It has been suggested that both atmospheric states (Tziperman et al. 1995, 1997, 1998; Harrison and Vecchi 1999; Vecchi and Harrison 2003) and oceanic states (An and Wang 2001; Xiao and Mechoso 2009; Ham et al. 2012a) are important for the ENSO phase-locking in winter.

Earlier studies proposed that the seasonal variation of anomalous atmospheric response to the ENSO-related SST change is a key element in the dynamics of ENSO phase-locking (Philander 1983; Tziperman et al. 1995, 1997, 1998; Harrison and Vecchi 1999; Vecchi and Harrison 2003). The magnitude of ENSO-related atmospheric response, which is often referred to as air-sea coupling strength, is the weakest in boreal winter over the equatorial Pacific, and it determines the timing of ENSO peak by controlling the amplitude of oceanic waves. Several studies pointed out that this seasonally-varying air-sea coupling strength is closely linked to the meridional migration of ENSO-related surface wind anomalies (Harrison and Vecchi 1999; Vecchi and Harrison 2003, 2006; Spencer 2004; Lengaigne et al. 2006; Lengaigne and Vecchi 2010;

Y.-G. Ham
Faculty of Earth Systems and Environmental Sciences,
Chonnam National University, Kwangju, South Korea

J.-S. Kug (✉)
School of Environmental Science and Engineering, Pohang
University of Science and Technology, Pohang, South Korea
e-mail: jskug1@gmail.com

McGregor et al. 2012). The downwelling Kelvin waves, which amplify the El Niño SST, are excited in the western to central Pacific due to anomalous equatorial westerly forcing, and propagate to the east. It normally takes 2–3 months to reach the eastern Pacific. To the west of the anomalous westerly wind forcing, oceanic Rossby waves are generated. The Rossby waves reach the eastern Pacific in about 6 months as upwelling Kelvin waves, which brings to an end of the El Niño growth (Suarez and Schopf 1988). Two or three months after the end of the calendar year, the SST growth due to the downwelling Kelvin waves becomes weakest due to the minimum coupling strength; however, the SST damping due to the reflected upwelling Kelvin waves is still increasing because they were excited 6 months earlier when the coupling strength was increasing in time. In this way, the upwelling Kelvin waves become dominant toward the end of the calendar year, and the peak of El Niño locks to the seasonal cycle (Tziperman et al. 1997, 1998).

Xiao and Mechoso (2009) showed that the seasonal variation of the coupling strength is closely related to seasonal evolution of the sea-surface temperature (SST). They pointed out that the strong air-sea coupling strength during the boreal spring is partly caused by the seasonal warming of the eastern tropical Pacific basin from January to April. It is the reduced zonal climatological gradient related to the seasonal warming over the eastern Pacific to shift the convective activity to the east, then the local wind response to the ENSO can be amplified to enhance the tropical air-sea coupling strength (Ham and Kug 2012; Kug et al. 2012).

Similarly, the oceanic basic state was reported to be crucial for the ENSO phase-locking. Ham et al. (2012a; hereafter H12) argued that the variation of the zonal SST gradient and resultant thermocline change over the eastern Pacific can determine the timing of the ENSO peak by regulating the strength of zonal advective and thermocline feedbacks. In addition, some studies noted that the advection of heat content anomalies by the seasonally varying mean circulation may also be important to the ENSO phase-locking (Vintzileos et al. 1999; Guilyardi et al. 2003).

Even with these progresses in understanding the mechanism of the ENSO phase-locking, it is not yet conclusive as to what controls the phase-locking of ENSO in Coupled General Circulation Models (CGCM). In particular, many state-of-the-art CGCMs still have a problem in simulating the phase-locking of the ENSO (Joseph and Nigam 2006; Wittenberg et al. 2006; Ham et al. 2012a). Joseph and Nigam (2006) showed that only two of the six CGCMs utilized in their study have ENSO phase-locking close to the observed distribution. H12 pointed out that five of the 14 CGCMs utilized in their study have an ENSO peak in

summer unlike the observations, that is, the strong SST variance appears during summertime. There is only modest improvement in simulating ENSO phase-locking even in Coupled Model Intercomparison Project Phase 5 (CMIP5) models (Bellenger et al. 2013). This is also an important issue for successful ENSO forecast, since the difficulties in correctly simulating the ENSO seasonal variation in the tropical Pacific leads to deteriorating prediction skill (Jin and Kinter 2009).

To improve our knowledge on the ENSO phase-locking and use it for a successful ENSO simulation in CGCMs, we examine which factors are crucial for obtaining a realistic ENSO phase-locking in CMIP archives in this study. This is a follow-up work of H12, in which we mainly focused on the ENSO phase-locking in a single coupled model (i.e., GFDL CM2.1) with different physical parameter values and 14 CMIP3 models. Here, we use both CMIP3 and CMIP5 archives (a total of 42 models), and analyze more general perspectives in multi-model framework.

This paper is organized as follows. Section 2 provides a description of the data and models used in this study. The oceanic and atmospheric basic states that are related to the simulation of the ENSO phase-locking are investigated in Sect. 3, and the role of the ENSO-related fields in ENSO phase-locking simulation is examined in Sect. 4. The summary and discussions are presented in Sect. 5.

2 Model outputs and data sets

We analyzed the historical runs by 21 CGCMs that participated in CMIP3, and another 21 models from CMIP5. The historical runs in CMIP3 are all from 1850 to 2000 under changing greenhouse gases (i.e., CO₂, N₂O, CH₄, CFCs). The historical runs in CMIP5 are done from 1850 to 2005, under changing solar-volcanic forcing in addition to changing greenhouse gases. Information on these models is summarized in Table 1.

For comparison with the model results, we use observed atmospheric and oceanic data. The SST data is the improved Extended Reconstructed Sea Surface Temperature version 2 (ERSST V.2; Smith and Reynolds 2004) from the National Climate Data Center. The monthly data of surface wind and zonal wind stress are from the EC-MWF 40 Year reanalysis (ERA-40; Uppala et al. 2005). The periods of ERSST V.2 and ERA-40 data used are 52 and 43 years from 1959 to 2010 and from 1959 to 2001, respectively. The monthly precipitation is the Modern ERA Retrospective-analysis for Research and Applications (MERRA; Rienecker et al. 2011) from 1980 to 2010. For sub-surface temperature, we use the NCEP Global Ocean Data Assimilation System (GODAS; Behringer and Xue 2004) from 1981 to 2010.

Table 1 Description of models used in this study

Archive	Modeling group	Model number in Fig. 1a	CMIP ID	Integration period (year)	Number of ensemble member
CMIP5	IPSL	1	IPSL-CM5A-MR	156	1
	CSIRO-QCCCE	2	CSIRO-Mk3-6-0	156	10
	IPSL	3	IPSL-CM5A-LR	156	4
	NOAA/GFDL	6	GFDL-ESM2 M	145	1
	MRI	8	MRI-CGCM3	156	3
	Hadley Centre/Met Office	9	HadGEM2-ES	145	4
	NOAA/GFDL	10	GFDL-CM3	145	1
	Hadley Centre/Met Office	13	HadGEM2-CC	145	1
	INM	14	INM-CM4	156	1
	MPI-M	20	MPI-ESM-LR	156	3
	NCC	22	NorESM1-M	156	1
	NOAA/GFDL	23	GFDL-ESM2G	145	1
	CCSR, JAMSTEC	26	MIROC-ESM	156	3
	CCSR, JAMSTEC	29	MIROC5	156	1
	NCAR	32	CCSM4	156	1
	BCCR	34	BCC-CSM1.1	156	3
	CCCMA	35	CanESM2	156	5
	CSIRO-BOM	36	ACCESS1-0	156	1
	NASA/GISS	37	GISS-E2-R	156	2
	LASG	40	FGOALS-g2	110	1
Météo-France	42	CNRM-CM5	156	9	
CMIP3	CSIRO-QCCCE	4	CSIRO-Mk3.5	130	3
	INM	5	INM-CM3.0	131	1
	NOAA/GFDL	6	GFDL-CM2.1	140	3
	NCAR	11	NCAR_PCM1	110	4
	CSIRO-QCCCE	12	CSIRO-Mk3.0	130	3
	NOAA/GFDL	15	GFDL-CM2.0	140	3
	MPI	16	MPI_ECHAM5	140	4
	BCCR	17	BCCR-BCM2.0	150	1
	Hadley Centre/Met Office	18	UKMO-HadGEM1	140	2
	CCCMA	19	CCCMA_CGCM_3.1_t63	151	1
	NCAR	21	NCAR-CCSM3.0	140	4
	CCSR, JAMSTEC	24	MIROC3.2_HIRES	101	1
	LASG	25	IAP_FGOALS-g1.0	150	3
	IPSL	27	IPSL-CM4	141	1
	MRI	28	MRI-CGCM2.3.2a	150	5
	University of Bonn, KMA	30	MIUB_ECHO-G	141	5
	Météo-France	31	CNRM-CM3	140	1
	CCSR, JAMSTEC	33	MIROC3.2_MEDRES	151	3
	Hadley Centre/Met Office	38	UKMO-HadCM3	140	2
	CCCMA	39	CCCMA_CGCM_3.1	151	5
INGV	41	INGV_ECHAM4	100	1	

3 Role of basic states in ENSO phase-locking

The ENSO phase-locking during the boreal winter can be seen clearly in Nino3 index during the El Nino events using

lag composite analysis (Neelin et al. 2000), or the standard deviation of the Nino3 index for each calendar month (An and Wang 2001). Similarly, to check the ENSO phase-locking, we first check the simulated standard deviation of

the Nino3 index for each calendar month (Fig. 1a, b). For the CMIP5 models, the multi-model ensemble (MME) values show similar behavior with the observed, namely, the ENSO peaks in December and January, even though the seasonal variation in these models is weaker than the observed. On the other hand, the minimum of Nino3 index is delayed about 1 or 2 months than the observed. In addition, some models show ENSO peak in April or September, implying that simulating realistic ENSO phase-locking is still problematic in some CGCMs. In the CMIP3 models (Fig. 1b), the MME values exhibit peak phase during the boreal winter; however, the seasonal variation of the Nino3 standard deviation is even weaker than that in the CMIP5 models. Some of these models have ENSO peak in the boreal summer (i.e., July, August, or September).

Even though the variation of Nino3 is seen in all these models, it is hard to quantify each model's fidelity in simulating the ENSO phase-locking. To easily access a model performance in terms of ENSO phase-locking, we define an ENSO phase-locking performance index as the correlation between standard deviations of Nino3 SST anomaly (SSTA) for each model and observation in each

calendar month. Hereafter, the ENSO phase-locking performance index is denoted as the PP index. We confirmed the PP index in this study shows significant correlation (0.61) with the phase-locking index in Bellenger et al. (2013) using ratio of variability between OND and MAM season, and the general conclusion is not changed which index is used. Also, the PP index based on the RMSE between the model's monthly variability and that in observation also shows strong correlation with PP index based on the correlation, therefore, the detail definition of PP index does not change the general conclusion of this study.

Figure 1c shows the PP index of CMIP3 and CMIP5 archives, with 34 models exhibit positive PP index, while eight show negative PP index. Among the models with positive PP index, only 14 models (33 % of the total 42 models) show values higher than the 95 % confidence level (i.e. about 0.6), implying that these state-of-the-art CGCMs still have problems in simulating realistic ENSO phase-locking. The numbers of the models whose PP index is larger than 0.6 are eight in CMIP5 and six in CMIP3, implying that the models participated in CMIP5 do not show significant improvement in terms of ENSO phase-

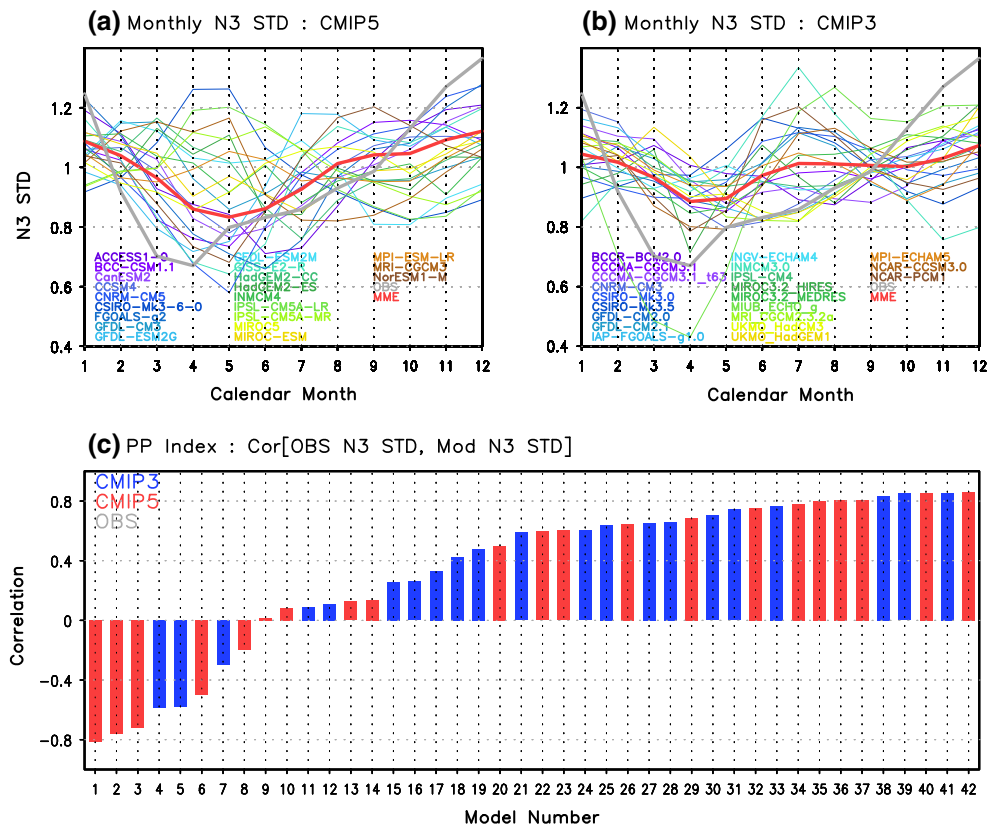
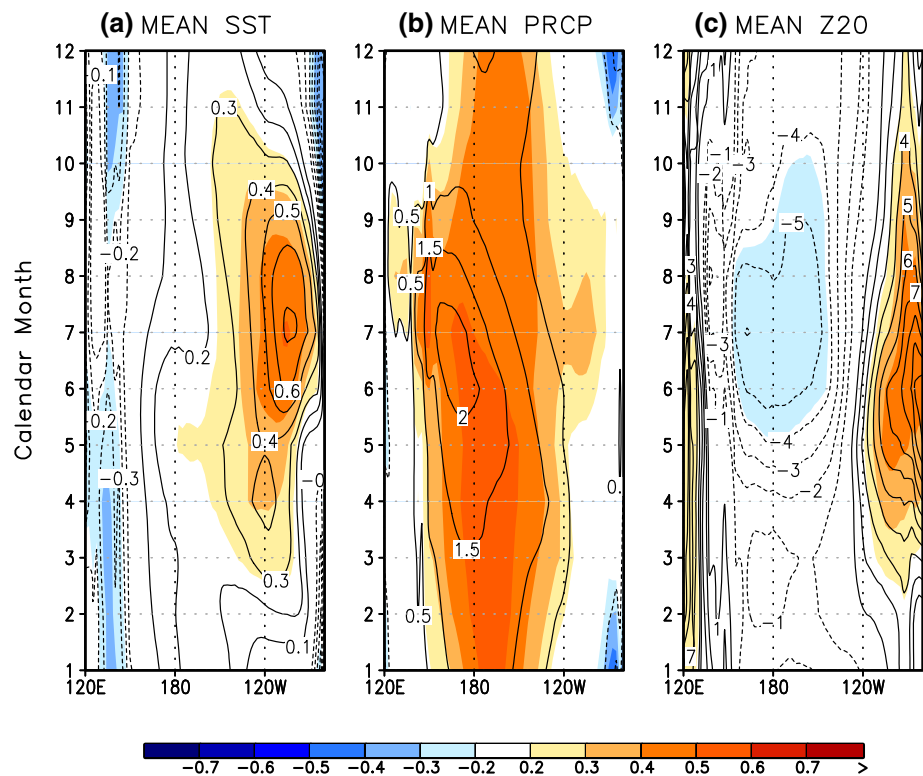


Fig. 1 Monthly standard deviation (STD) of Nino3 index in **a** CMIP5 and **b** CMIP3. The *red curve* denotes the multi-model ensemble (MME) value, and the *light gray* one denotes the observation. **c** Phase-locking Performance (PP) index of 42 climate models,

defined as the correlation between observed and simulated monthly Nino3 standard deviation. The monthly STD of Nino3 index in **a** and **b** is normalized by STD of Nino3 using all months

Fig. 2 The correlation (shading) and regression (contour) between the PP index and monthly-mean equatorial (5°S–5°N) **a** SST, **b** precipitation, and **c** thermocline depth



locking compared to the earlier CMIP3 models. Among the eight negative PP index models, five of them are from the CMIP5 archives, while three are from the CMIP3.

In order to examine which basic states are important for simulating realistic ENSO phase-locking, we analyzed inter-model differences in climatological states based on the PP index. First, the anomalous PP index for each model from MME value, and anomalous mean state deviated from MME value is calculated. Then, we calculated the correlation and regression between two variables (i.e. PP index and anomalous mean state) using the 42 CGCMs. Then, the regression values denote the additional mean state to the MME which favors high PP index. That is, the ENSO phase-locking in terms of seasonal variation of Nino3 magnitude becomes more similar to the observed as the PP index increases, and the regressed field can be interpreted as the basic state which favors the simulation of a realistic ENSO phase-locking.

Figure 2 shows the correlation and regression coefficients between climatological equatorial SST, precipitation, and 20 °C isotherm depth (i.e., Z20) in each calendar month and PP index. In SST, robust positive signals are clear over the equatorial eastern Pacific during the boreal summer. This indicates that the models with a warmer SST climatology over the eastern Pacific during summertime tend to simulate the ENSO phase-locking better. In other words, a colder eastern Pacific during

summertime is linked to a poor simulation of the phase-locking.

About the role of eastern Pacific SST in the ENSO phase-locking, H12 argued that it modulates ENSO-related feedbacks by changing zonal SST gradient. That is, the climate models with colder climatological eastern Pacific SST during the boreal summer (i.e., with strong zonal SST gradient) have a stronger zonal advective feedback (An and Jin 2001). In addition, the enhanced zonal SST gradient also intensifies the thermocline feedback by leading stronger climatological easterly and resultant shallower thermocline depth over the eastern Pacific (An and Wang 2001). The results in this study support the argument in H12 that the boreal-summer climatological SST over the equatorial eastern Pacific is important to the realistic simulation of ENSO phase-locking in CGCMs by controlling the oceanic feedbacks.

The climatological SST warming over the eastern Pacific is linked to the enhanced mean precipitation in the central Pacific (Fig. 2b). During the boreal summer, the regression coefficient is as large as 2 mm/day, and it gradually decreases in the following seasons. It is interesting that the positive precipitation signal is still significantly correlated with PP index during the boreal winter without significant SST signal. It implies that the atmospheric basic state plays a critical role for the realistic simulation of ENSO phase-locking during the boreal

winter, while both oceanic and atmospheric basic states play some roles during the boreal summer. We will focus on the boreal winter in the next section.

According to H12, a deeper climatological thermocline depth over the eastern Pacific during the boreal summer (Fig. 2c) helps to simulate realistic ENSO phase-locking. H12 mentioned that the deepening of the thermocline is related to the weakening of the thermocline feedback and suppresses the summer SST variability. Note that the thermocline shoaling over the central Pacific is likely to have less impact on the ENSO variability, because the thermocline feedback is less active there (Kang et al. 2001).

As shown in Fig. 2, more distinctive signals in the basic state appear during the boreal summer. To examine this in more detail, Fig. 3 shows spatial distributions of the regression and correlation of precipitation, SST, and thermocline depth with respect to the PP index during June–August (JJA). Consistent with Fig. 2, there are positive SST anomalies over the eastern Pacific, while negative signals are robust over the off-equatorial western and central Pacific. As the SST warming over the eastern

Pacific will weaken the overlying trade winds and ultimately lead to the deepening of thermocline depths in the eastern equatorial Pacific, and shoaling in the off-equatorial central Pacific (Fig. 3c).

Similar to the equatorial Z20 signal, the off-equatorial western-central Pacific (between 10°S and 10°N) Z20 shoals, while polewards of this region a deepening of Z20 is seen. These Z20 signals can be also explained by the changes in the atmospheric basic states. There is a negative precipitation signal over the off-equatorial regions. As a Gill-type Rossby wave response to the off-equatorial negative atmospheric forcing (i.e. negative precipitation signal), there are anti-cyclonic flows over the sub-tropical (i.e., poleward of 10°N and 10°S) western Pacific. Downwelling (upwelling) related to the anti-cyclonic flow leads to positive Z20 over the sub-tropical region. In the off-equatorial region (equatorward of 10°N and 10°S), there are cyclonic flow in the response to the equatorial positive heating and off-equatorial negative forcing, which can lead to equatorial thermocline shoaling.

Interestingly, we found that the climate models with realistic ENSO phase-locking tend to have smaller biases

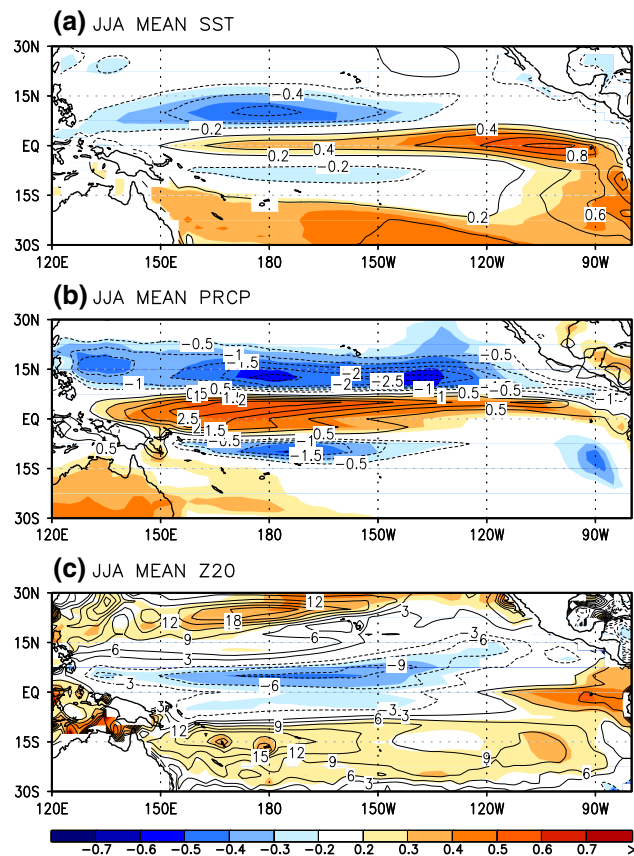


Fig. 3 The correlation (*shading*) and regression (*contour*) between the PP index and JJA-mean **a** SST, **b** precipitation, and **c** thermocline depth of all 42 models over the tropical Pacific

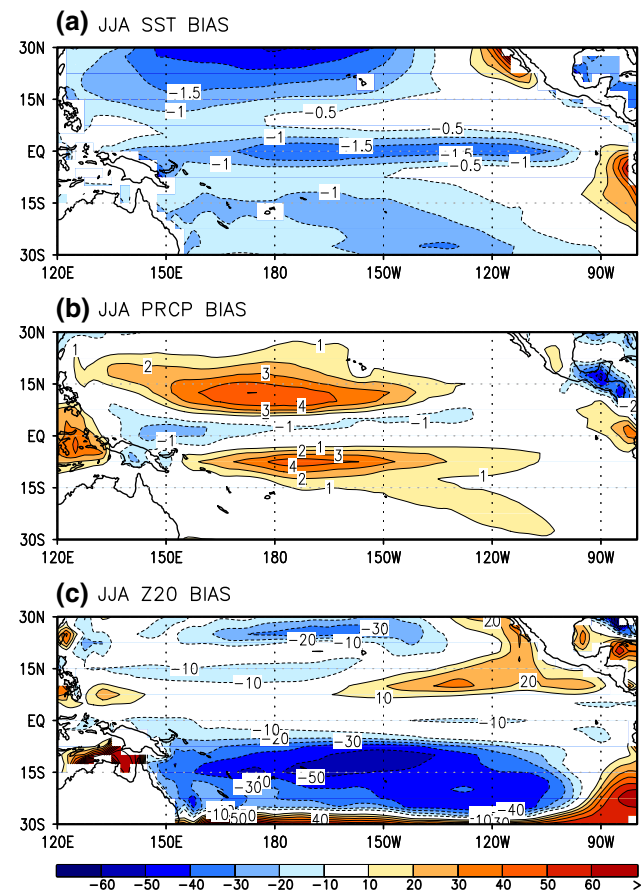


Fig. 4 The JJA MME bias of **a** SST, **b** precipitation, and **c** thermocline depth of all 42 models over the tropical Pacific

in their equatorial mean states. Figure 4 shows the MME bias of precipitation, SST, and thermocline depth during JJA. It is clear that the spatial pattern of MME bias generally opposes to the PP index-regressed basic fields, which means the climatology in the high PP-index models tends to have smaller mean bias. For example, the MME bias of SST is negative over the equatorial regions (Wittenberg et al. 2006; Ham et al. 2012b), while there is a positive mean SST signal in the high PP-index models (Figs. 3a, 4a). The precipitation biases show negative and positive values over the equatorial band and off-equatorial regions, respectively, which is almost opposite to the high PP-index climatology (Figs. 3b, 4b). For the Z20, there is a strong negative bias between 15 and 30°S, and there is a weak negative bias over the equatorial eastern Pacific (Figs. 3c, 4c). These results suggest that the poor simulation of the ENSO phase-locking is partly attributed to poor simulation in the summer basic state.

So far, we have only examined the basic state that favors the simulation of realistic ENSO phase-locking. These results may indicate that the equatorial basic state during the boreal summer is critical in simulating the ENSO phase-locking. The SST warming over the eastern Pacific during the boreal summer weakens the zonal temperature gradient; therefore, it reduces summer ENSO amplitude by reducing the zonal advective feedback. At the same time, a weaker zonal SST gradient reduces the climatological easterly over the equator and flattens the tropical thermocline, which also leads weak SST variability by reducing the thermocline feedback.

In addition to the oceanic state, the atmospheric basic state is significantly related to the ENSO phase-locking during the boreal summer by modulating atmospheric responses to ENSO-related SST forcing. Kim et al. (2011) pointed out that the increases in the mean precipitation can lead to stronger atmospheric responses to ENSO-related SST forcing over the equatorial Pacific, thanks to enhanced climatological convection. It means that the increased summer-mean precipitation can intensify the air-sea coupling strength in this season. This increased air-sea coupling allows SST anomalies to continue growing during the boreal summer, thus ensuring no ENSO peak during this season.

To measure the air-sea coupling strength, Fig. 5 shows the regression of equatorial zonal wind stress onto the Nino3 index for each calendar month in the observation and MME. In the observation, the wind stress response over the central Pacific is the strongest during the boreal autumn. Even though there is a second peak in March, it is partly canceled by the negative zonal wind stress response over the western Pacific. This negative zonal wind stress over the western Pacific is related to the subtropical anticyclonic flow, which is known to be crucial for ENSO transition (Wang et al. 2000). As a result, the coupling

strength over the tropical Pacific (defined as averaged ENSO-related wind stress anomaly over the region of 120°E–90°W and 5°S–5°N) is minimum in January and maximum in September (Ham et al. 2012a). The weakened downwelling Kelvin waves after the September maximum coupling strength, act to weaken SST growth several months later. On the other hand, the SST damping due to the reflected upwelling Kelvin waves is still increasing up until about 6 months the September peak where the growth due to the downwelling Kelvin wave is overwhelmed by the damping of the reflected upwelling Kelvin wave, thus leading to the event end (Tziperman et al. 1997). Therefore, the seasonal dependency of the coupling strength is critical for ENSO phase locking.

The MME result is generally consistent with the observation. The response over the central Pacific is the strongest in October and November, and the weakest in March. Since the negative response over the western Pacific is quite weak in the MME, especially during November–February, the minimum of the coupling strength over the Pacific is in March.

In the models with dry bias over the equatorial Pacific during the boreal summer, the ENSO phase-locking is expected to be simulated poorly due to the unrealistic ENSO-related atmospheric feedback. To examine the impact of summer-mean precipitation on the coupling strength, we calculated the averaged coupling strength in the models with dry climatology over the equatorial central Pacific during JJA. For the models with dry climatology, we selected 21 models (i.e., half of the total models) whose climatological precipitation over central Pacific (i.e., 140°E–150°W, 5°S–5°N) is low. Hereafter, we define these models as “Dry JJA CP” models. In the “Dry JJA CP” models, the biggest difference from the MME is the weakening (increasing) in the coupling strength over the central Pacific during the JJA (MAM). This feature is also shown in the model with low PP index models (not shown).

As expected from previous studies, the air-sea coupling strength during boreal summer season is weaker in “Dry JJA CP” models than that in MME, while the air-sea coupling strength from boreal spring season is stronger in “Dry JJA CP” group. As the air-sea coupling strength increases, the SST growth due to the Kelvin wave also enhances with 2 months lag, which means the strengthening of summer SST variability to help to lead the ENSO peak at summer. However, note that the absolute amplitude of air-sea coupling strength is still stronger in boreal summer season than that in spring season, which implies other factors like oceanic feedback plays a crucial role to determine the ENSO peak season in “Dry JJA CP” models as mentioned before.

In this section, we mainly focused on the boreal summer, when the oceanic basic state is significantly related to

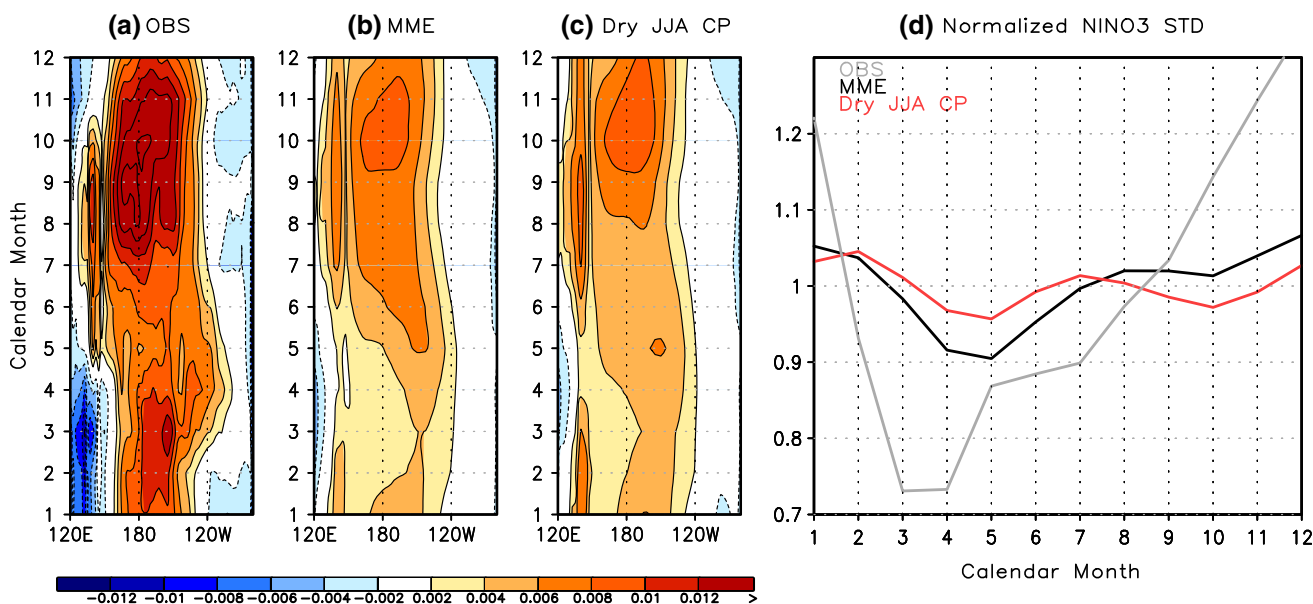


Fig. 5 The regressed equatorially-averaged (5°S–5°N) zonal wind stress anomaly onto the Nino3 index ($\text{N/m}^2/^\circ\text{C}$) in each calendar month from **a** observation, **b** MME, and **c** “Dry JJA CP” model composite. **d** The Nino3 standard deviation in the observation (*light*

gray), MME (black), and “Dry JJA CP” model composite (*red*) for each calendar month. To focus on the seasonal variation, values in **(d)** are normalized by the total Nino3 standard deviation using all months

the simulation of ENSO phase-locking. Our findings confirm the results in H12 that the strengthening of zonal SST gradient enhances zonal advective feedback and ENSO amplitude during the boreal summer. In addition, the strengthening of zonal SST gradient results in strong seasonal-mean easterly and shallow thermocline, which helps to amplify the ENSO amplitude during the boreal summer by intensifying the thermocline feedback. In addition, the climatological SST cooling over the eastern Pacific weakens the summer coupling strength to weaken the growth of ENSO SST after few months later to lead the summer peak.

Even though the boreal summer is highlighted in terms of oceanic basic state, some models give poor simulation of the phase-locking, resulted from a biased boreal-winter basic state. As indicated by Fig. 2b, intensity of boreal winter-mean precipitation is important in simulating realistic ENSO phase-locking, while boreal winter-mean SST and Z20 are not much relevant to the simulation of ENSO phase-locking. In the next section, we will investigate how the boreal winter-mean atmospheric state affects the simulation capability of ENSO phase-locking in CGCMs.

4 Role of ENSO-related fields during boreal winter in ENSO phase-locking

Since positive boreal winter-mean precipitation is linked to the realistic simulation of ENSO phase-locking (Fig. 2b), and since this change in the atmospheric basic state can

modulate ENSO by changing ENSO-related atmospheric responses (Jin 1997), we will now examine how ENSO-related anomalous patterns in SST, precipitation are different among the climate models with respect to the degree of ENSO phase-locking via the PP index. To do this, firstly, we calculate a linear regression of DJF precipitation and SST with respect to the Nino3 index for each of these models. Note that the regression is the response to the unit change of the Nino3 index, so that the ENSO forcing in the linear regression can be thought to be similar among all these climate models. Then, we calculate the correlations between PP index and Nino3-regressed fields, to quantify the pattern of ENSO-related anomalies in the realistic simulation of ENSO phase-locking.

Figure 6 shows the correlations between ENSO-related fields and PP index using the 42 climate models. It is clear that there are some meaningful relations between ENSO-related patterns and PP index. For SST, there are significant negative SST signals over the western Pacific. Since the MME value of Nino3-regressed SST shows positive values over the western Pacific (contour in Fig. 6a), a negative signal indicates that the model with realistic ENSO phase-locking tends to have weaker positive SST anomalies during El Niño events over the western Pacific. In the observation, there is a negative SST anomaly over the western Pacific during the El Niño due to the Ekman pumping induced by the anticyclonic flow (Weisberg and Wang 1997a, b, Kug et al. 2005). However, in the models there is a common problem that the positive SST anomaly

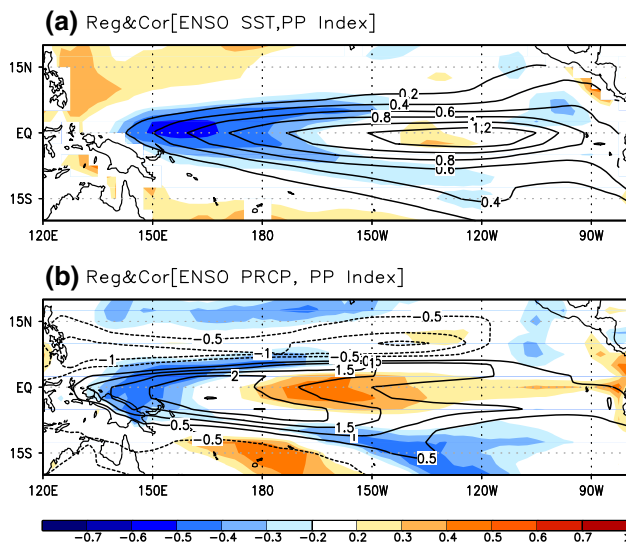


Fig. 6 Shading denotes the correlation between the PP index and Nino3-regressed **a** DJF SST and **b** DJF precipitation. Contours denote the MME values of Nino3-regressed **a** DJF SST and **b** DJF precipitation

extends too far to the west, so there is almost a basin-wide warming over the tropical Pacific during the El Niño (Davey et al. 2002; AchutaRao and Sperber 2006; Ham et al. 2012b). Therefore, the negative SST signal in Fig. 6a implies that the model that has less westward extension of positive ENSO-related SSTA tends to have a more realistic ENSO phase-locking. This means that the models with more realistic spatial pattern of the ENSO tend to simulate realistic ENSO phase-locking.

Consistent with the negative SST signal over the western Pacific, there is a negative correlation between PP index and ENSO-related precipitation pattern over the equatorial western Pacific. In addition, there is a positive precipitation signal over the central Pacific. Since the MME precipitation response to the El Niño SST forcing is in-between these dipole signals of the precipitation, the high PP-index models tend to have eastward-shifted ENSO-related precipitation. In other words, the model tends to simulate ENSO phase-locking poorly when its precipitation response during the El Niño is confined over the western Pacific.

To investigate the anomalous SST evolution in more detail, we compare the monthly standard deviation of equatorial SST in the observation, MME, and the models with excessive positive ENSO-related SSTA over the western Pacific (i.e., “WP ENSO” models) in Fig. 7. We calculate Nino3-regressed SST pattern during DJF, and select 10 CGCMs whose area-averaged regression coefficient over the equatorial western Pacific (150–180°E, 5°S–5°N) is the largest (i.e. larger than 0.7) to define “WP ENSO” models. In the observation, the SST variability

shows an obvious peak in the boreal winter, which is stronger over the eastern Pacific between 140 and 120°W. The overall spatial pattern of the MME is similar to that of the observed, but the maximum SST variability is slightly shifted to the west.

However, the SST variability in the “WP ENSO” models is quite different from the observed. During the boreal winter, the SST peak is located in the western Pacific; On the other hand, the SST variability in the eastern Pacific is quite weak, and shows its peak during the boreal summer. The standard deviation of the normalized Nino3 also shows consistent results, that is, the Nino3 variability peaks during the boreal summer in the “WP ENSO” models. This implies that the strong SST variability over the western Pacific during boreal winter season is linked to the failure of ENSO phase-locking due to the excessive atmospheric wind response over the equatorial western Pacific.

Figure 8 shows the regression of the 850-hPa zonal wind anomaly onto the DJF Nino3 index and seasonal wind difference in the observation, MME, and the “WP ENSO” models from the boreal fall to the subsequent spring. In the observation, there are westerly anomalies over the central Pacific during the boreal fall. The maximum of these westerly anomalies is located at the equator during SON. However, the westerly is increased (decreased) at the south (north) of the equator during DJF, which implies the movement of the westerly to the southern hemisphere. Previous studies argued that this southward shift of El Niño-related westerly plays a critical role in having the ENSO peak in the boreal winter (Harrison and Vecchi 1999; Vecchi and Harrison 2003, McGregor et al. 2012). Similarly, McGregor et al. (2013) focused on the southward shift of zonal wind stress anomalies during boreal winter season to lead ENSO peak by controlling the equatorial heat content. In addition, there are easterly differences at equatorial western Pacific during DJF (Fig. 8b), and the difference becomes bigger during MAM (Fig. 8c), which also leads to transition of El Niño (Kug and Kang 2006, Kug et al. 2006a, b). This easterly difference is closely related to the rapid establishment and development of the Philippine Sea anticyclone in these seasons (Wang et al. 2000).

In the MME, the seasonal difference of the zonal wind anomaly at DJF season from SON season is simulated to some extent, even though the overall wind response during the El Niño is weak; that is, the westerly peak is in-between the equator and 5°N during SON, and the positive (negative) signal in seasonal wind difference from SON to DJF season is shown around 5°S. (5°N) The wind difference over the equatorial western Pacific is negative as shown in observation with weaker amplitude. However, the low-wind response in the “WP ENSO” models exhibits

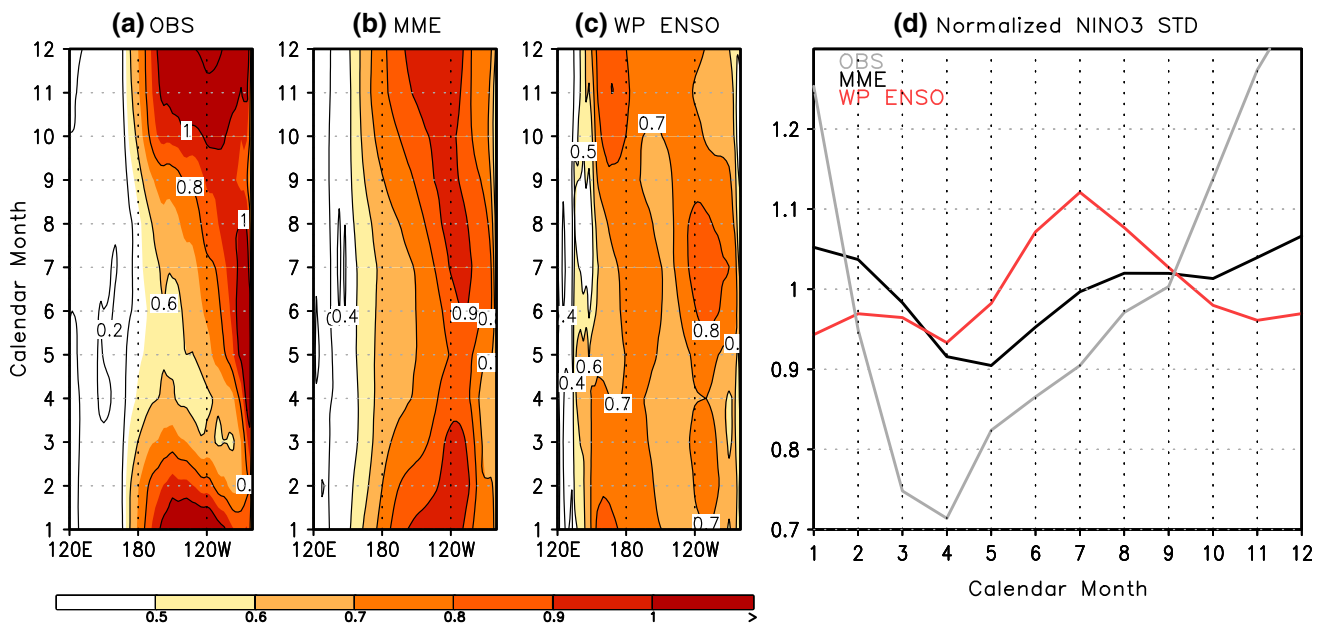


Fig. 7 Monthly-mean standard deviation of equatorial (5°S – 5°N) SSTa in **a** the observation, **b** MME, **c** “WP ENSO” group. **d** The Nino3 standard deviation in the observation (*light gray*), MME

(*black*), and “WP ENSO” model composite (*red*) for each calendar month. To focus on the seasonal variation, values in **(d)** are normalized by the total Nino3 standard deviation using all months

systematic difference from that in the MME or observation. That is, even though there is some southward shift, the positive signal in the seasonal difference map shifts to the north compared to the observation or MME. Also, the negative signal over the north of the equator at the western Pacific is weaker than the MME or observation. The easterly signal over the equatorial western Pacific is weakest. This implies that the peak of the westerly is still on the equator during DJF.

It might be due to the positive equatorial SSTa over the equatorial western Pacific acts to enhance local convective activity and resultant additional low-level westerly winds. These results in excessive equatorial low-level response during the boreal winter, which leads to a growing SSTa over the eastern Pacific, instead of an ENSO peak, during the boreal winter. In other words, the weakening of the low-level westerly related to the southward shift of westerly over the central Pacific, and the development of the Philippine Sea anticyclone is not clear in the “WP ENSO” models, which might be responsible for the failure of winter ENSO peak. Note that this feature is also clear in low-PP-index models (not shown).

The remaining question is whether or not there is a possible connection between strong SST variability over the western Pacific and winter-mean precipitation shown in Fig. 2b. That is, the models with poorly simulated ENSO phase-locking tend to show dry bias over the central Pacific during the boreal winter (Fig. 2b) and it is related to the excessive positive ENSO-related SSTa over the western

Pacific (Fig. 6a). To confirm this, Fig. 9 presents the climatological precipitation during DJF in the observation, MME composite, and the “WP ENSO” composite. In the observation, the Intertropical convergence zone (ITCZ) in the North Pacific and the South Pacific convergence zone (SPCZ) over the southwestern Pacific are clear. The magnitude of the precipitation over the western Pacific is generally greater, reaching about 5 mm/day at the dateline. For the MME, the overall precipitation pattern is similar to the observed; however, the SPCZ is more zonally elongated due to double ITCZ problem (Lin 2007) and the magnitude of the precipitation over the central-eastern Pacific is weaker than the observed (i.e., 3.5 mm/day at the dateline). Instead, the magnitude of the precipitation over the western Pacific is greater, which means that the climatological convective activity in the MME is confined over the western Pacific. The lack of DJF-mean convection over the central-eastern Pacific is much severe in the “WP ENSO” models (Fig. 9c), with the climatological convective activity being less than 2 mm/day over the central Pacific during DJF. The correlation coefficient between SST amplitude over the western Pacific (150°E – 180°E , 5°S – 5°N) and climatological central Pacific precipitation (140°E – 150°W , 5°S – 5°N) during DJF season is -0.52 , which confirms the clear relationship between the western Pacific SST variability and climatological precipitation.

Watanabe et al. (2011) suggested that the (dry) bias in the eastern Pacific shifts the atmospheric responses of ENSO-related SSTa westward. Similarly, Ham and Kug

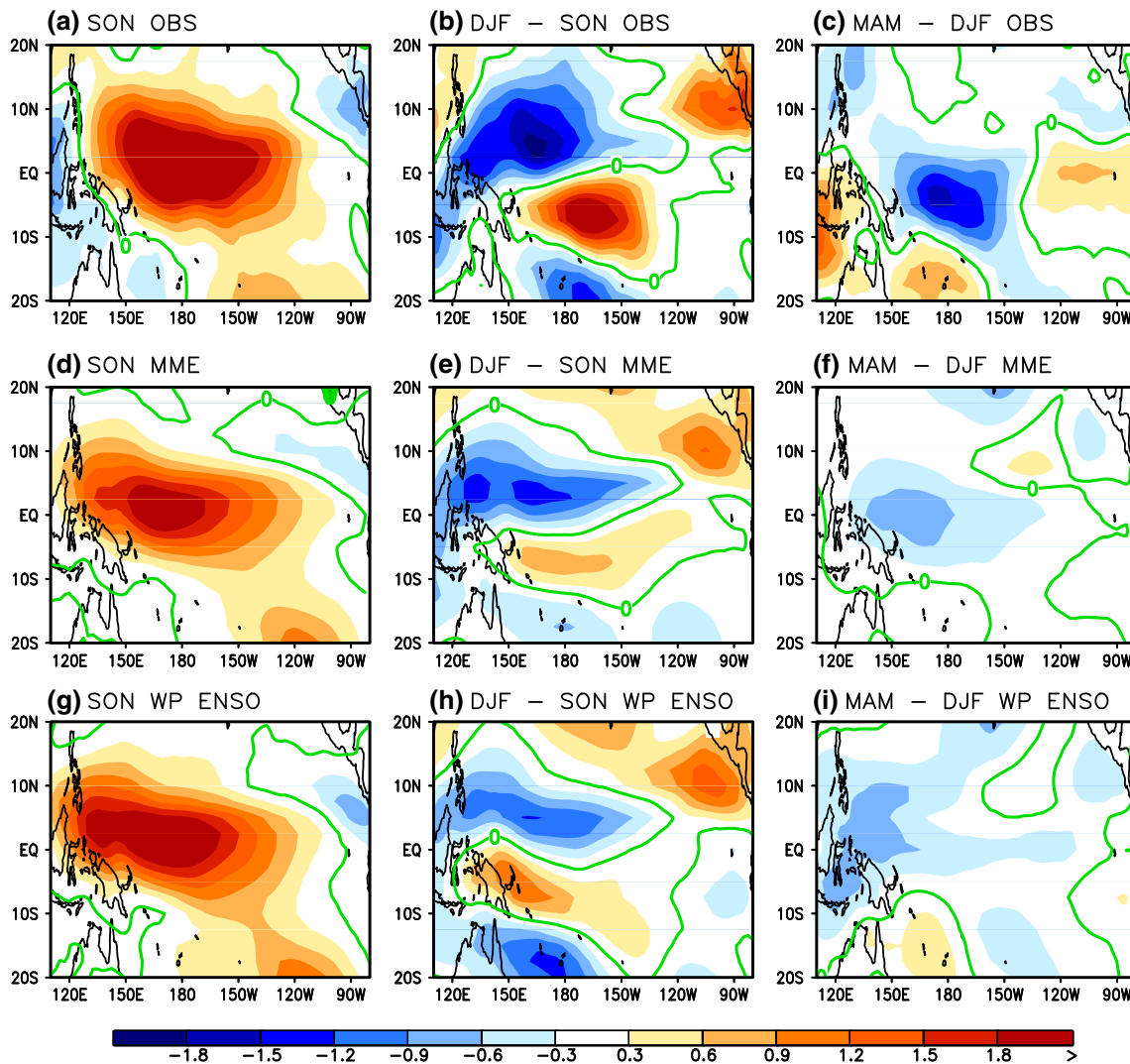


Fig. 8 The regression of 850-hPa zonal wind anomaly onto DJF Niño3 index in the observation (*top panels*), MME (*mid panels*), and “WP ENSO” composite (*low panels*) during SON (*left panels*), composite during DJF season minus that during SON season (*mid*

panels), and the composite during the following MAM season minus that during previous DJF season (*right panels*). Note that the *green line* denotes the zero contour

(2012) showed that the location of ENSO-related atmospheric responses depends on the spatial distribution of the winter-mean convection; that is, once there is a dry bias over the equatorial central Pacific, the ENSO-related anomalous convection is reduced over the central Pacific, therefore, the ENSO-related convective anomaly is also confined over the western Pacific. That is why the ENSO-related precipitation with respect to the PP index shows a dipole pattern over the equatorial western-central Pacific. This excessive convective anomaly over the western Pacific prevents the southward shift of the westerly wind from SON to DJF season; as a result, the coupling strength remains strong for sustaining the ENSO-related SSTA during boreal winter season.

5 Summary and conclusions

In this study, ENSO phase-locking in winter is examined using 42 models in the CMIP3 and CMIP5 archives. Based on the monthly standard deviation of Niño3 index, we showed that many models still have problems in simulating realistic ENSO phase-locking. The low PP-index models tend to simulate cold eastern Pacific SST with shallower thermocline, which acts to amplify zonal advection and thermocline depth feedbacks during the boreal summer. It is also revealed that the bias of high PP index models during the boreal summer is relatively small compared to that of the low PP index models over the tropical Pacific, implying that the realistic simulation of the climatological

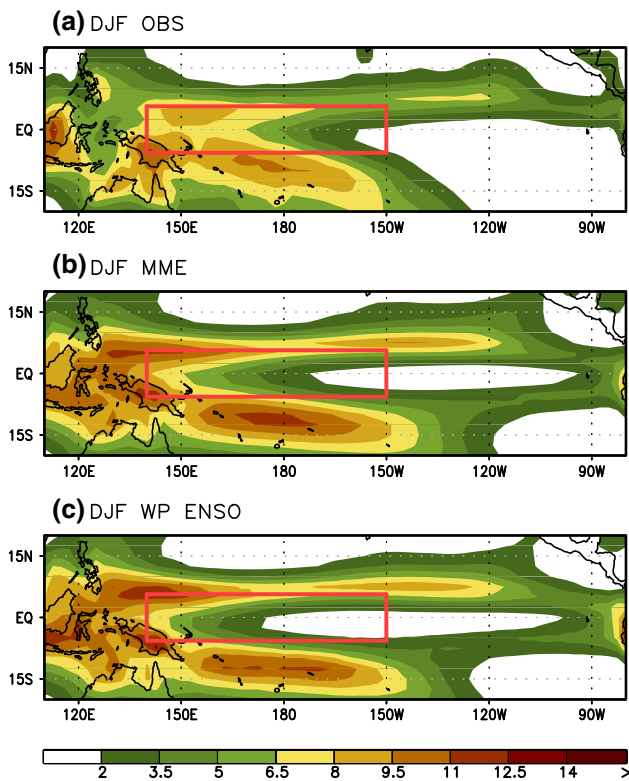


Fig. 9 Climatological precipitation during DJF in **a** the observation, **b** MME composite, and **c** “WP ENSO” composite. The *red box* denote the area over 140°E–150°W, 5°S–5°N

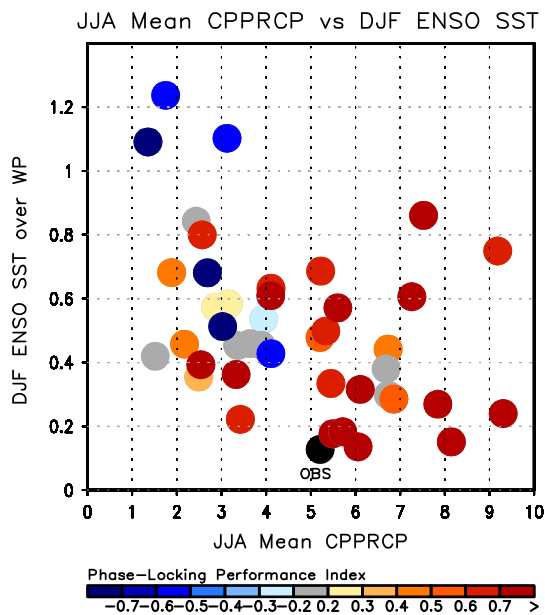


Fig. 10 Scatter diagram between JJA-mean precipitation over the central Pacific (140°E–150°W, 5°S–5°N; x-axis) and DJF-mean SST anomalies over the western Pacific regressed onto the Nino3 index (150–180°E, 5°S–5°N; y-axis) in the 42 CMIP CGCMs. The PP index is denoted by *colored dots* with *blue* (negative PP index), *gray* (PP index is nearly zero), and *red* (positive PP index), and the observation is denoted by a *black dot*. See the *color bars* for details

fields helps to simulate winter ENSO peak. In addition, the seasonal variation of air-sea coupling strength also affects the ENSO phase-locking.

During the boreal winter, the relationship between the PP index and mean oceanic states (i.e. SST or thermocline depth) is not clear. Instead, some models simulate excessive SST variability over the western Pacific, which prevent from the realistic seasonal-locking. The excessive positive ENSO SSTA over the western Pacific leads to strong convection anomalies and is related to the low-level westerly over equatorial western Pacific. This keeps the tropical coupling strength strong, which means that the ENSO-related SSTA continues to grow during the boreal winter. This, in part, can be caused by the dry biases over the central Pacific during the boreal winter by confining ENSO-related atmospheric responses over the equatorial western Pacific.

To summarize our findings in this study, Fig. 10 shows the scatter diagram between the summer-mean precipitation over the central Pacific (140°E–150°W, 5°S–5°N) and DJF-mean SST anomalies over the western Pacific regressed onto the Nino3 index (150–180°E, 5°S–5°N). In the observation, the JJA-mean precipitation over the central Pacific is about 5 mm/day, and about half of the 42 models have similar degrees of the JJA-mean precipitation. The simulated ENSO-related SSTA is generally stronger than the observed. This bias is related to the excessive westward extension of ENSO-related SSTA in the climate models as mentioned earlier.

It is obvious that the high PP-index models have relatively high mean-JJA precipitation. Most of the climate models whose summer-mean central Pacific precipitation is higher than 5 mm/day exhibits a PP index higher than 0.6. On the other hand, all of the models with negative PP-index values have summer-mean precipitation less than 5 mm/day over the central Pacific. Among them, some models have very low negative PP index when their ENSO-related SSTA over the western Pacific is excessively strong in winter. For example, for the three models whose ENSO-related SSTA over the western Pacific in winter is larger than one, their PP index values are less than –0.5. When the DJF ENSO over WP is between 0.3 and 1, then there is various PP index value. When the DJF ENSO over WP is less than 0.3, all the most shows strong positive PP index. The correlation between PP index and DJF ENSO SST over western Pacific is 0.52, which is significant with 99 % confidence level.

One can be curious about the role of heat flux feedbacks on ENSO phase-locking as pointed out some previous studies (H12; Bellenger et al. 2013). To check this point, we calculate the correlation between the PP index and Nino3-regressed shortwave radiation and latent heat flux (not shown). It is found that the model with high PP index tends to have less incoming solar radiation during the

boreal winter season El Niño event. As the less incoming solar radiation is related to the weak El Niño amplitude, it is hard to say that the strong negative atmospheric in high PP-index models is a cause of the realistic ENSO phase-locking (i.e. strong SST variability during the boreal winter season). Rather the strong negative atmospheric feedback in high PP-index models is a result of realistic ENSO phase-locking. There was no significant correlation between the PP index and ENSO-regressed latent heat flux. In short, we conclude that the atmospheric heat flux feedback is not a crucial factor to determine the quality of ENSO phase-locking in CMIP models.

It is worth pointing out the dry biases over the central-eastern Pacific is closely linked to the spatial distribution of the SPCZ shown in Fig. 9. In the observation, the SPCZ is elongated from north-west to south-east over the western Pacific; therefore, the western part of the SPCZ contributes to more equatorial precipitation. However, when the SPCZ is too elongated zonally over the off-equatorial Southern Hemisphere as in the “WP ENSO” models, it does not contribute to the equatorial winter-mean precipitation. It implies that the spatial pattern of the SPCZ can play a role in simulating realistic ENSO phase-locking. This is consistent with the recent study of McGregor et al. (2012), which emphasizes the seasonal evolution of the SPCZ, even though they focused on the role of momentum damping through SPCZ-related circulation change.

Acknowledgment This work was funded by the Korea Meteorological Administration Research and Development Program under grant CATER 2012-3042.

References

- AchutaRao K, Sperber KR (2006) ENSO Simulation in coupled ocean–atmosphere models: are the current models better? *Clim Dyn* 27:1–15
- An S-I, Jin F-F (2001) Collective role of thermocline and zonal advective feedbacks in the ENSO mode. *J Clim* 14:3421–3432
- An S-I, Wang B (2001) Mechanisms of locking the El Niño and La Niña mature phases to boreal winter. *J Clim* 14:2164–2176
- Behringer DW, Xue Y (2004) Evaluation of the global ocean data assimilation system at NCEP: the Pacific Ocean. Eighth symposium on integrated observing and assimilation systems for atmosphere, ocean and land surface, AMS 84th annual meeting, Washington State Convention and Trade Center, Seattle, Washington, pp 11–15
- Bellenger H, Guilyardi E, Leloup J, Lengaigne M, Vialard J (2013) ENSO representation in climate models: from CMIP3 to CMIP5. *Clim Dyn*. doi:10.1007/s00382-013-1783-z
- Davey M, Huddleston M, Sperber K et al (2002) STOIC: a study of coupled model climatology and variability in tropical ocean regions. *Clim Dyn* 18:403–420
- Guilyardi E, Delecluse P, Gualdi S, Navarra A (2003) Mechanisms for ENSO phase change in a coupled GCM. *J Clim* 16:1141–1158
- Ham Y-G, Kug J-S (2012) How well do current climate models simulate two-types of El Niño? *Clim Dyn* 39:383–398. doi:10.1007/s00382-011-1157-3
- Ham Y-G, Kug J-S, Kim D, Kim Y-H, Kim D-H (2012a) What controls phase-locking of ENSO to boreal winter in coupled GCMs? *Clim Dyn*. doi:10.1007/s00382-012-1420-2
- Ham Y-G, Kang I-S, Kim D, Kug J-S (2012b) El-Niño southern oscillation simulated and predicted in SNU coupled GCMs. *Clim Dyn* 38:2227–2242. doi:10.1007/s00382-011-1171-5
- Harrison DE, Vecchi GA (1999) On the termination of El Niño. *Geophys Res Lett* 26:1593–1596
- Jin F-F (1997) An equatorial ocean recharge paradigm for ENSO. Part I: conceptual model. *J Atmos Sci* 54:811–829
- Jin EK, Kinter JL III (2009) Characteristics of tropical Pacific SST predictability in coupled GCM forecasts using the NCEP CFS. *Clim Dyn* 32:675–691. doi:10.1007/s00382-008-0418-2
- Jin F-F, Neelin D, Ghil M (1994) ENSO on the devil’s staircase. *Science* 264:70–72
- Joseph R, Nigam S (2006) ENSO evolution and teleconnections in IPCCs twentieth-century climate simulations: realistic representation? *J Clim* 19:4360–4377
- Kang I-S, An S-I, Jin F-F (2001) A systematic approximation of the SST anomaly equation for ENSO. *J Meteorol Soc Jpn* 79:1–10
- Kim D, Jang Y-S, Kim D-H, Kim Y-H, Watanabe M, Jin F-F, Kug J-S (2011) ENSO sensitivity to cumulus entrainment in a coupled GCM. *J Geophys Res Atmos* 116:D22112. doi:10.1029/2011JD016526
- Kug J-S, Kang I-S (2006) Interactive feedback between the Indian Ocean and ENSO. *J Clim* 19:1784–1801
- Kug J-S, Kang I-S, Jhun J-G (2005) Western Pacific SST prediction with an intermediate coupled model. *Mon Weather Rev* 133:1343–1352
- Kug J-S et al (2006a) Role of the ENSO-Indian Ocean coupling on ENSO variability in a coupled GCM. *Geophys Res Lett* 33:L09710. doi:10.1029/2005GL024916
- Kug J-S, Ben PK, Kang I-S (2006b) Interactive feedback between ENSO and the Indian Ocean in an interactive coupled model. *J Clim* 19:6371–6381
- Kug J-S, Ham Y-G, Lee J-Y, Jin F-F (2012) Improved simulation of two types of El Niño in CMIP5 models. *Environ Res Lett* 7. doi:10.1088/1748-9326/7/3/039502
- Lengaigne M, Vecchi GA (2010) Contrasting the termination of moderate and extreme El Niño events in coupled general circulation models. *Clim Dyn* 35:299–313
- Lengaigne M, Boulanger JP, Menkes C, Spencer H (2006) Influence of the seasonal cycle on the termination of El Niño events in a coupled general circulation model. *J Clim* 19:1850–1868. doi:10.1175/JCLI3706.1
- Lin JL (2007) The double-ITCZ problem in IPCC AR4 coupled GCMs: ocean-atmosphere feedback analysis. *J Clim* 20:4497–4525. doi:10.1175/JCLI4272.1
- McGregor S, Timmermann A, Schneider N, Stuecker MF, England MH (2012) The effect of the South Pacific convergence zone on the termination of El Niño events and the meridional asymmetry of ENSO. *J Clim* 25:5566–5586
- McGregor S, Ramesh N, Spence P, England MH, McPhaden MJ, Santoso A (2013) Meridional movement of wind anomalies during ENSO events and their role in event termination. *Res Lett Geophys*. doi:10.1002/grl.50136
- Neelin JD, Jin F-F, Syu H-H (2000) Variations in ENSO phase locking. *J Clim* 13:2570–2590. [http://dx.doi.org/10.1175/1520-0442\(2000\)013<2570:VIEPL>2.0.CO;2](http://dx.doi.org/10.1175/1520-0442(2000)013<2570:VIEPL>2.0.CO;2)
- Philander SG (1983) El Niño-Southern Oscillation phenomena. *Nature* 302:295–301

- Rienecker MM et al (2011) MERRA—NASA's modern-era retrospective analysis for research and applications. *J Clim*. doi:[10.1175/JCLI-D-11-00015.1](https://doi.org/10.1175/JCLI-D-11-00015.1)
- Smith T, Reynolds R (2004) Improved extended reconstruction of SST (1854–1997). *J Clim* 17:2466–2477
- Spencer H (2004) Role of the atmosphere in the seasonality of El Niño. *Geophys Res Lett* 31:L24104. doi:[10.1029/2004GL021619](https://doi.org/10.1029/2004GL021619)
- Suarez MJ, Schopf PS (1988) A delayed action oscillator for ENSO. *J Atmos Sci* 45:3283–3287
- Tziperman E, Cane MA, Zebiak S (1995) Irregularity and locking to the seasonal cycle in an ENSO prediction model as explained by the quasi-periodicity route to chaos. *J Atmos Sci* 52:293–306
- Tziperman E, Zebiak SE, Cane MA (1997) Mechanisms of seasonal—ENSO interaction. *J Atmos Sci* 54:61–71
- Tziperman E, Cane MA, Blumenthal B (1998) Locking of El Niño peak time to the end of the calendar year in the delayed oscillator picture of ENSO. *J Clim* 11:2191–2203
- Uppala SM et al (2005) The ERA-40 re-analysis. *Q J R Meteorol Soc* 131:2961–3012. doi:[10.1256/qj.04.176](https://doi.org/10.1256/qj.04.176)
- Vecchi G, Harrison D (2003) On the termination of the 2002–03 El Niño event. *Geophys Res Lett* 30(18):1964. doi:[10.1029/2003GL017564](https://doi.org/10.1029/2003GL017564)
- Vecchi GA, Harrison DE (2006) The termination of the 1997–98 El Niño. Part I: mechanisms of oceanic change. *J Clim* 19:2633–2646
- Vintzileos A, Delecluse P, Sadourny R (1999) On the mechanisms in a tropical ocean–global atmosphere coupled general circulation model. Part II: interannual variability and its relation to the seasonal cycle. *Clim Dyn* 15:63–80
- Wang B, Wu R, Fu X (2000) Pacific–East Asian teleconnection: how does ENSO affect East Asian climate? *J Clim* 13:1517–1536
- Watanabe M, Chikira M, Imada Y, Kimoto M (2011) Convective control of ENSO simulated in MIROC. *J Clim* 24:543–562
- Weisberg RH, Wang C (1997a) A western Pacific oscillator paradigm for the El Niño–Southern Oscillation. *Geophys Res Lett* 24:779–782
- Weisberg RH, Wang C (1997b) Slow variability in the equatorial west-central Pacific in relation to ENSO. *J Clim* 10:1998–2017
- Wittenberg AT, Rosati A, Lau N-C, Ploshay JJ (2006) GFDL's CM2 global coupled climate models. Part III: tropical Pacific climate and ENSO. *J Clim* 19:698–722
- Xiao H, Mechoso CR (2009) Seasonal cycle–El Niño relationship: validation of hypotheses. *J Atmos Sci* 66:1633–1653